

XVI. PLASMA ELECTRONICS*

Prof. L. D. Smullin	J. F. Clarke	D. L. Morse
Prof. H. A. Haus	P. Edmonds	A. A. Offenberger
Prof. A. Bers	S. A. Evans	L. M. Petrie, Jr.
Prof. W. D. Getty	T. J. Fessenden	S. Puri
Prof. P. Penfield, Jr.	E. T. Gerry	C. G. Robertson
Prof. D. J. Rose	R. Hancox	P. S. Spangler
Prof. T. H. Dupree	B. A. Hartenbaum	G. Theodoridis
Prof. L. M. Lidsky	C. F. G. Hsi	E. Thompson
Prof. E. P. Gyftopoulos	H. Y. Hsieh	P. B. Ulrich
R. R. Bartsch	G. I. Kachen	M. T. Vlaardingerbroek
W. L. Brasser	B. Kusse	C. E. Wagner
R. J. Briggs	M. A. Lieberman	H. L. Witting
T. S. Brown	L. N. Lontai	J. C. Woo
	J. D. Mills	

RESEARCH OBJECTIVES AND SUMMARY OF RESEARCH

1. Plasmas for Electrical Energy Conversion

This group is concerned with the synthesizing or design of particular plasma systems to perform specific functions. The research program described below is concerned primarily with the plasma as a component of a power generator: either controlled thermonuclear fusion or magnetohydrodynamic. To implement this program, we are studying several methods of producing and containing dense, hot plasmas. We are also concerned with the collective behavior of plasmas of finite dimensions, and are studying possible means of energy extraction. Thus we are led to the investigation of waves in plasma waveguides and their stability, and of millimeter oscillations induced by drifting plasmas in semiconductors.

(a) Beam-Plasma Discharge

During the past year we have made considerable progress toward gaining a detailed understanding of the dynamics of the beam-plasma discharge (BPD). From study of the time behavior of the radiofrequency spectrum radiated by the discharge, we have clarified our ideas about the interaction mechanisms, and we have evidence of direct excitation of the ions by the beam, at the ion plasma frequency. Our studies of the loss mechanisms have uncovered a "rotating spoke" instability. The newest beam-plasma discharge device has a hollow, high-perveance, electron beam. It generates a plasma density $> 2 \times 10^{13}/\text{cm}^3$ in a neutral gas background of $2 \times 10^{12}/\text{cm}^3$, X-rays with energy > 100 kv with a voltage of 7-10 kv. During the coming year we shall pay particular attention to the excitation of ion plasma oscillations as a means of heating the ions.

L. D. Smullin, W. D. Getty

(b) Electron-Cyclotron Resonant Discharge

We have placed in operation a medium-power device. Pulsed RF power 50 kw peak, 50-100 watts avg, is used to excite a cylindrical cavity, 15 inches in diameter, at

*This work was supported in part by the National Science Foundation (Grant G-24073); and in part by Purchase Order DDL BB-107 with Lincoln Laboratory, a center for research operated by Massachusetts Institute of Technology, with the support of the U.S. Air Force under Contract AF 19(628)-500.

(XVI. PLASMA ELECTRONICS)

3000 mc. The average x-radiation just outside the cavity is ~ 5 r/m, and energies > 1 Mev are observed. Diamagnetic probe signals indicate that a relatively high β plasma is produced. Low-frequency oscillations (~ 10 - 30 mc) are radiated by the plasma during the interpulse period.

During the coming year we shall study the parametric behavior of the electron-cyclotron resonance discharge (ECRD) with special emphasis on the mechanisms for transferring energy from the electrons to the ions.

L. D. Smullin, T. J. Fessenden

(c) Beam-Induced Ion Plasma Oscillations

Experiments on the beam-plasma discharge have indicated that the electron beam can induce oscillations at ω_{pi} , if the electrons are hot enough. In these new experiments we are using a medium-power electron-cyclotron resonance discharge (ECRD) to produce a plasma with hot electrons. Into this plasma we fire an electron beam, and we shall examine the spectrum of the induced oscillations.

L. D. Smullin, M. T. Vlaardingerbroek, M. A. Lieberman

(d) Theory of Active and Passive Anisotropic Waveguides

This research will proceed along two lines.

(i) Development of small-signal energy and momentum-conservation principles that are applicable to the linearized equations of anisotropic waveguides in the absence of loss will be undertaken to obtain criteria for the stability or amplifying nature of the waves in these systems.

(ii) Analysis of specific waveguides of present interest, and determination of their dispersion characteristics will be carried out.

The dispersion characteristics may also be used to test the general criteria obtained from the conservation principles.

A. Bers, H. A. Haus, P. Penfield, Jr.

2. Highly Ionized Plasma and Fusion Research

Studies that are applicable to controlled nuclear fusion assume many forms. Our activities, for the most part, are involved with plasmas: plasma kinetic theory, plasma production by injection, nonadiabatic particle motions, stability and turbulence, and interaction with coherent radiation. Our other activities (energy extraction and tritium regeneration through a surrounding blanket, superconducting magnetic-field structures for plasma confinement), while motivated by the thought of controlled fusion, have wider applicability.

(a) Interaction of Coherent Radiation and Plasmas

Study of the following physical problems, by means of pulsed high-intensity laser beams, continues:

(i) Thomson scattering from free electrons in an electron beam, as a diagnostic tool for study of beam structure;

(ii) Thomson scattering from free electrons in an almost fully ionized plasma (ion density 10^{13} - $10^{14}/\text{cm}^3$, neutral density 10^{11} - $10^{12}/\text{cm}^3$);

- (iii) Photoionization of excited atoms in a plasma, and related phenomena;
- (iv) Measurement of the plasma correlation structure, by means of scattering through angles $\theta \approx$ (laser wavelength/ 2π Debye length); and
- (v) Light-suppression and light-collection techniques to optimize the methods involved in experiments of this general nature.

E. Thompson, L. M. Lidsky, D. J. Rose

(b) Plasma Kinetic Theory

Our research in plasma kinetic theory is concentrated in two general areas. The first is concerned with the derivation of "reasonably" simple but "reasonably" exact equations to provide a complete description of plasma behavior. The starting point has usually been a set of generalized hierarchy equations that includes the transverse electromagnetic field. The second phase of the program is directed toward obtaining interesting solutions to the fundamental equations to second order in the plasma parameter. General formulas for the approach to equilibrium, including expressions for radiation emission and absorption, have been derived.

T. H. Dupree

(c) Nonadiabatic Motion of Particles

Our studies of charged-particle trapping by injection into nonadiabatic systems are being extended to include the general problem of weakly nonadiabatic motion in various magnetic structures of practical interest. This work will include study of particle "unwinding" devices, and minimum-field plasma-confinement configurations.

L. M. Lidsky, D. J. Rose

(d) Plasma Turbulence and Stability

The structure of plasma columns in axial magnetic fields is being studied theoretically and experimentally, with a view toward applying concepts of turbulent motion to the analysis of their behavior. New minimum-field confinement configurations will be applied to these plasma columns and possibly to differently produced plasmas, to decrease the level of turbulent instability at the plasma-vacuum interface.

D. J. Rose, L. M. Lidsky

(e) Ion Beam

With the advent of Lorentz dissociation of excited molecular beams and Lorentz ionization of excited atomic beams, we are extending our low-divergence high-current ion-beam studies to include measurements of the efficiency of production of excited atomic and molecular beams and their subsequent ionization and dissociation.

E. Thompson

(f) Superconducting Magnet

Modifications of our superconducting magnet assembly to remove a thermal contact have been completed. Analysis of, and introspection concerning, the present design of large superconducting magnets, based upon experience gained thus far, lead us to quite different design concepts. A new configuration will be detailed during the coming year. A propos of superconducting magnet systems, in general, we remark that the newer minimum-field configurations for more stable plasma confinement are exceedingly

(XVI. PLASMA ELECTRONICS)

expensive in terms of magnetic field energy; the plasma is also kept relatively remote from the field sources. These requirements, in our opinion, will be satisfied by superconducting magnet systems, and by no other kind.

D. J. Rose, L. M. Lidsky

(g) Thermonuclear-Blanket Studies

We have shown that if confinement of a controlled-fusion plasma is possible, the nuclear and other facts of nature will permit regeneration of the tritium that is necessary for a D-T reaction, probably with a small safety margin. Principal extensions of this study will be

(i) Calculation of transport, neutron flux, and tritium regeneration in finite systems,

(ii) Experimental measurement of tritium production and of energy deposition (by means of gamma rays) in a cylindrical blanket mock-up with point neutron source,

(iii) Study of the physical and engineering feasibility (or nonfeasibility) of a fast pulsed controlled fusion system.

D. J. Rose, I. Kaplan

(h) Cesium Plasmas

Properties of low-energy cesium plasmas and formation of molecular ions through excited cesium-atom collisions have been investigated with promising results.^{1, 2}

Intermetallic adsorption systems have been studied during the past year. Heats of desorption and rates of emission of cesium and other metallic atoms and ions desorbed from partially covered surfaces have been derived theoretically.³⁻⁶ State functions for partially covered intermetallic surfaces have also been derived.

Work on these subjects, together with experimental studies of cesium ion-beam neutralization schemes, will continue.⁷

E. P. Gyftopoulos

References

1. H. Witting, Concentration of excited states in a low-energy cesium plasma, Quarterly Progress Report No. 70, Research Laboratory of Electronics, M.I.T., July 15, 1963, pp. 153-162.
2. H. Witting and E. P. Gyftopoulos, Volume Ionization Processes in Cesium Converters, presented at the Thermionic Converter Specialist Conference, Gatlinburg, Tennessee, October 7-9, 1963.
3. J. D. Levine and E. P. Gyftopoulos, Adsorption Physics of Metals Partially Coated by Metallic Films, Proc. Twenty-third Annual Conference on Physical Electronics, M. I. T., March 1963, pp. 239-249.
4. J. D. Levine, Adsorption Physics of Metals Partially Coated by Metallic Films, Ph.D. Thesis, Department of Nuclear Engineering, M. I. T., April 1963.
5. J. D. Levine and E. P. Gyftopoulos, Adsorption physics of metals partially coated by metallic particles, Part I - Desorption energies (to be published in Surface Science).

6. J. D. Levine and E. P. Gyftopoulos, Adsorption physics of metals partially coated by metallic particles, Part II – Desorption, vaporization and sublimation rates (to be published in Surface Science).

7. G. C. Theodoridis, Space-Charge neutralization experiment, Quarterly Progress Report No. 70, Research Laboratory of Electronics, M. I. T., July 15, 1963, pp. 164-167.

A. BEAM-PLASMA DISCHARGES

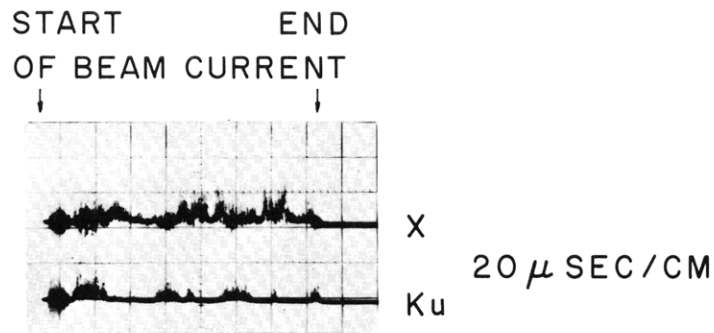
1. SYSTEM A: RADIOFREQUENCY SIGNALS RADIATED BY BEAM-PLASMA DISCHARGE

This report summarizes our observations of the radio frequencies emitted by the beam-plasma discharge. Three observations are particularly striking. First, strong microwave oscillations occur in several narrow bands of frequencies. Second, microwave frequencies continue to be emitted for as long as 15 μ sec after the beam pulse has ended. Third, strong VHF signals are observed at frequencies corresponding to the ion-plasma frequency.

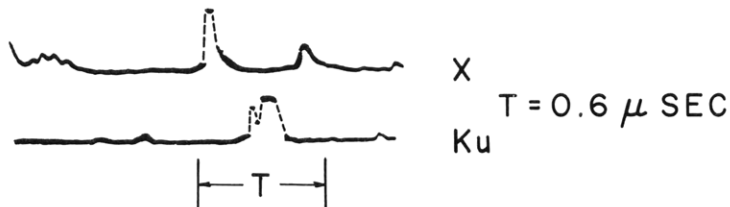
With either the wideband "video" detector or the narrow-band detector,¹ the microwave oscillations (5.5 kmc to 15 kmc) always appear as spikes in time. In many cases the duration of the spike appears to be limited by the bandwidth of the detector. Typically, a spike is 0.1-0.2 μ sec in duration, Fig. XVI-1b. At low magnetic fields (less than 250 gauss) the spikes occur more or less continuously during the entire beam-plasma discharge. At higher magnetic fields, the spikes occur in groups that vary in duration from 10 μ sec to 50 μ sec.¹ The strength of these oscillations varies along the axis. It is much stronger (10-100 times stronger) near the gun than at the collector, Fig. XVI-2. The same dependence has been found in both hydrogen and helium.

By comparing the outputs of two wideband "video" detectors that respond in different frequency ranges (the X-band detector covers a range of 7-10 kmc, the Ku-band detector covers a range of 10-14 kmc), it has been found that the oscillations in these two bands are anticoincident. Figure XVI-1c shows a correlogram of the Ku-signal and the X-signal. A 5- μ sec sample of the radio frequency is taken during each beam pulse, and the photograph is an exposure over 100 pulses. Figure XVI-1b shows a time-expanded view of the Ku-signal and X-signal, illustrating the anticoincident characteristics.

Using the spectrum analyzer, we found that strong microwave oscillations occur in several narrow bands of frequencies which are distinctly separated by intervals of very weak or no oscillations. A parametric mapping of the instantaneous frequency and intensity during the beam-plasma discharge is under way. Preliminary investigations show that at higher beam powers the bands move toward high frequencies, and that at high beam powers and high magnetic field, a rather intense continuum begins to build up.

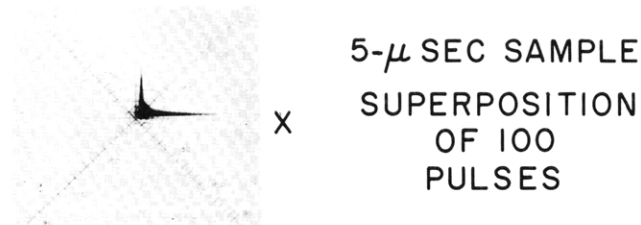


(a)



(b)

Ku



(c)

Fig. XVI-1. Oscillograms illustrating the general nature of the signals received by the Ku-band detector and the X-band detector. The experimental conditions for these three illustrations were not the same. (a) Groups of spikes received by the two detectors during the beam-plasma discharge. (b) Anti-coincidence of the two signals on an expanded time scale within a group.

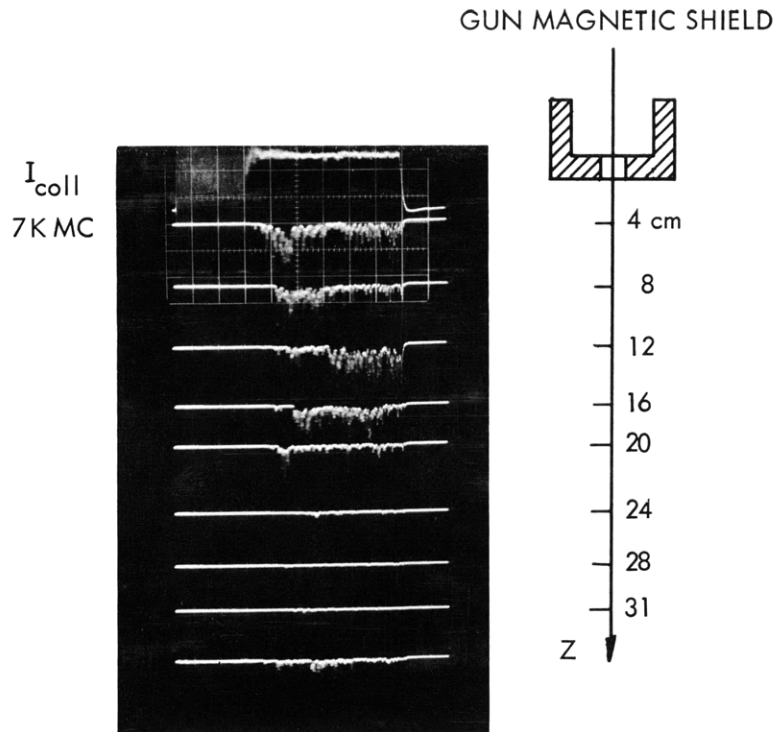


Fig. XVI-2. Oscillograms showing kmc oscillation amplitude as a function of axial position. The 7-kmc oscillation is picked up by a movable loop. The vertical calibrations are the same in the kmc oscillation traces except the last, which shows the 7-kmc signal at $z = 31$ cm when the vertical gain is increased by a factor of 10.

$P = 0.52 \mu \text{ Hg}$	$B_o = 280 \text{ gauss}$
$V_b = 5 \text{ kv}$	$I_{\text{coll}} = 0.26 \text{ amp}$
Time, $20 \mu\text{sec/cm}$	Hydrogen

a. Oscillations in the Absence of Beam Current

Up to $15 \mu\text{sec}$ after the beam current ended, frequencies in the ranges 100-300 mc and 6-10 kmc were observed. The oscillations always occur during the time at which the collector current represents a net ion current, Fig. XVI-3. The intensity of the oscillations during this "afterglow" is usually smaller than, but sometimes comparable to, the intensity of the oscillations during the beam-plasma discharge. In system A, one of the necessary conditions for observing these afterglow oscillations is that the magnetic field must be above a certain critical value, which is ~ 600 gauss.

The oscillations always occur as spikes. The oscillations observed both with the broadband "video" detectors and with the spectrum analyzer occur as trains of spikes. The number of spikes in the train varies from two to six. The spikes in the train occur

(XVI. PLASMA ELECTRONICS)

almost in regular intervals. The average period is approximately $2 \mu\text{sec}$. The general tendency, not always true, is for the intervals within the train to decrease with time. The train correlates well with a regular oscillation (whose period also varies in the

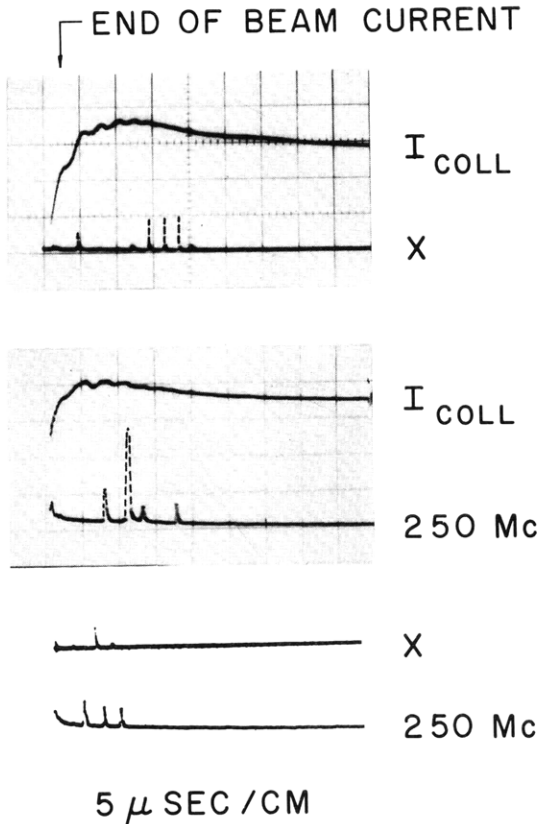


Fig. XVI-3. Oscillograms showing typical oscillations during the "after-glow."

$P = 0.55 \mu\text{Hg}$ $B_0 = 630 \text{ gauss}$
 $V_b = 5 \text{ kv}$ $I_{\text{coll}} = 0.24 \text{ amp}$
Hydrogen

same way as the train's) observed on a magnetic probe. The train does not correlate well with the fluctuations seen on a Langmuir probe. The train often occurs during the time when the net ion current on I_{coll} is flat. At the moment, the ensemble of pictures collected does not show a correlation between the spikes and the fluctuations in the light output. The last rf spike usually occurs within $15 \mu\text{sec}$ after the end of the beam current.

The afterglow oscillations indicate the presence of a highly anisotropic electron velocity distribution, which persists for $10\text{-}15 \mu\text{sec}$ after the beam is turned off. The existence of microwave oscillations implies an electron density of the order of 10^{12} ions/cc during this time. The VHF oscillations ($100\text{-}300 \text{ mc}$) lie in a range corresponding to the ion-plasma frequency. Presumably, they are both excited by an anisotropic velocity distribution of the electrons.²

H. Y. Hsieh

References

1. H. Y. Hsieh, Beam-plasma discharges. System A, Quarterly Progress Report No. 71, Research Laboratory of Electronics, M. I. T., October 15, 1963, pp. 114-115.

2. R. J. Briggs and A. Bers, Interaction of an electron beam with ions in a warm plasma of finite transverse dimensions, Quarterly Progress Report No. 71, Research Laboratory of Electronics, M. I. T., October 15, 1963, pp. 131-137.

2. SYSTEM B: ROTATIONAL INSTABILITY IN THE BEAM-PLASMA DISCHARGE

Space- and time-resolved light measurements indicate that a spoke of plasma rotates in a right-hand sense about the applied, axial magnetic field. The fields of view of the two telescopes¹ are shown in Fig. XVI-4. The oscillograms of the detected light output

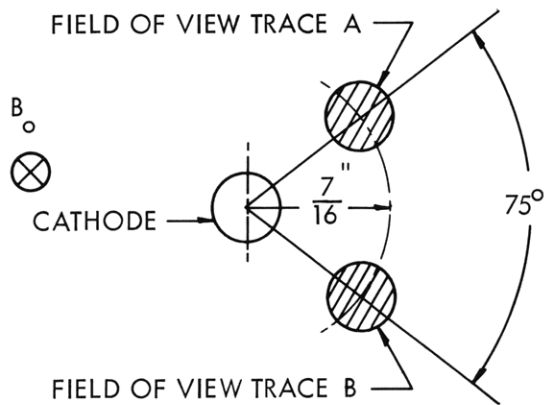


Fig. XVI-4. Fields of view of telescopes.

in Fig. XVI-5a show that trace A leads trace B by 0.2 period, which corresponds to the angular separation of the fields of view. The time lag between the two traces reverses with a reversal of the magnetic field. Oscillograms of probe current,¹ Fig. XVI-5b,

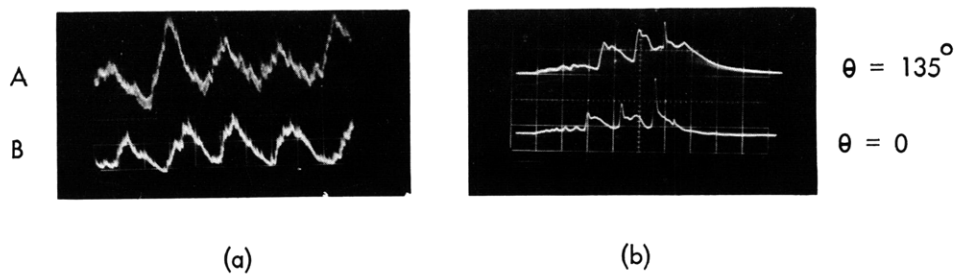


Fig. XVI-5. Rotational time lag.

(a) Light	(b) Probe currents
$p = 0.5 \mu \text{H}_2$	$p = 0.5 \mu \text{H}_2$
$B_0 = 540 \text{ gauss}$	$B_0 = 350 \text{ gauss}$
$V_0 = 7.2 \text{ kv}$	$V_0 = 7.2 \text{ kv}$
time, $10 \mu\text{sec/cm}$	time, $20 \mu\text{sec/cm}$

(XVI. PLASMA ELECTRONICS)

agree with the light measurements.

The instability begins above a critical magnetic field. Current to the beam collector for magnetic fields just below and above the critical field value is shown in Fig. XVI-6.

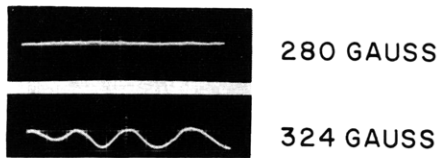


Fig. XVI-6. Beam collector current.

The critical magnetic field for onset of the instability is plotted in Fig. XVI-7.

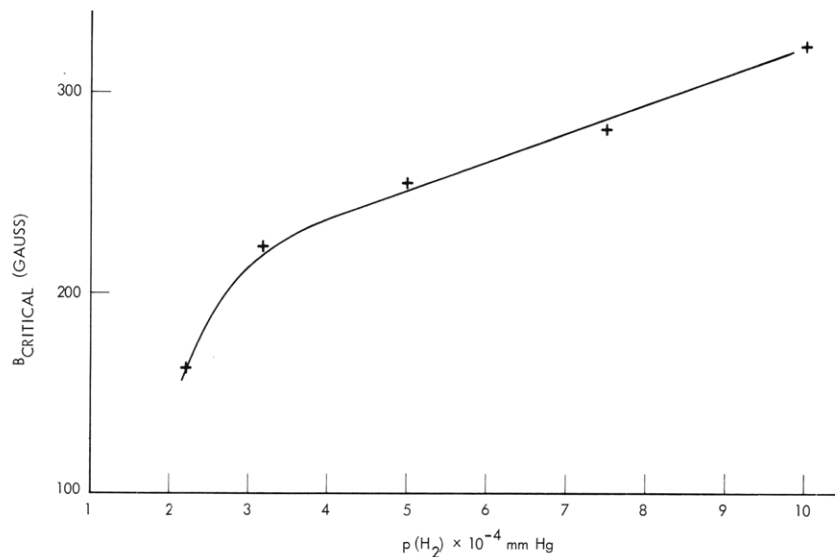


Fig. XVI-7. Critical magnetic induction for onset of instability.

Below approximately 550 gauss the oscillations on the beam collector are quite sinusoidal. Two electric probes at the same radial and azimuthal positions but at different axial positions indicate that the sinusoidal oscillations have no axial variation (Fig. XVI-7). The light and probe oscillograms of Fig. XVI-5 show that the variation must be $m = 1$ at low fields. Ion-current fluctuations on the beam-collector magnetic shield² occur 180° out of phase with ion-current fluctuations on the beam collector. This factor suggests an off-center rotation of a camlike plasma column about the beam collector, as shown in Fig. XVI-8.

Above approximately 550 gauss, probe signals at different axial positions are no

longer well correlated (Fig. XVI-9). Coincident with the decrease in the crosscorrelation between probe signals, the plasma currents and light become irregular, which suggests that the plasma has become "turbulent." The period of rotation is plotted as a function of

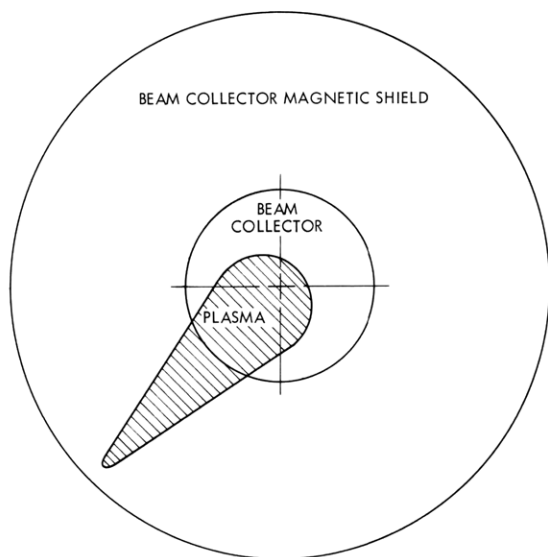


Fig. XVI-8. Plasma rotating off center.

magnetic field (at $0.5\text{-}\mu$ pressure) in Fig. XVI-10. The abrupt decrease in rotational speed is associated with the onset of "turbulence." From measurements of light at various radii from the axis we have estimated the radial electron-density variation.

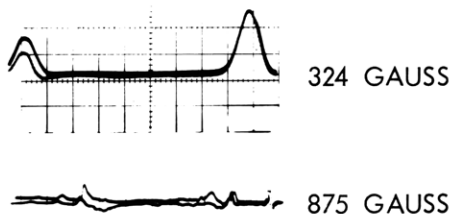


Fig. XVI-9. Axial variation in probe currents. Axial probe separation, 6.5 in.; $p = 0.4\ \mu\text{ H}_2$; $V_0 = 7.2\text{ kv.}$
Upper: time, $5\ \mu\text{sec/cm.}$ Lower: time, $20\ \mu\text{sec/cm.}$

The density e-folding length vs magnetic field at $0.5\text{-}\mu$ pressure is plotted in Fig. XVI-10. The e-folding length decreases linearly with B when the plasma is stable. The magnetic field no longer squeezes the plasma in so well when the coherent rotation sets in, and the plasma actually expands when turbulence occurs.

The rotational instability is a mechanism by which plasma is transported across the magnetic field. After the beam breakup, current to the wall electrodes² increases very slowly with time. Coincident with the appearance of the rotation, the wall current

(XVI. PLASMA ELECTRONICS)

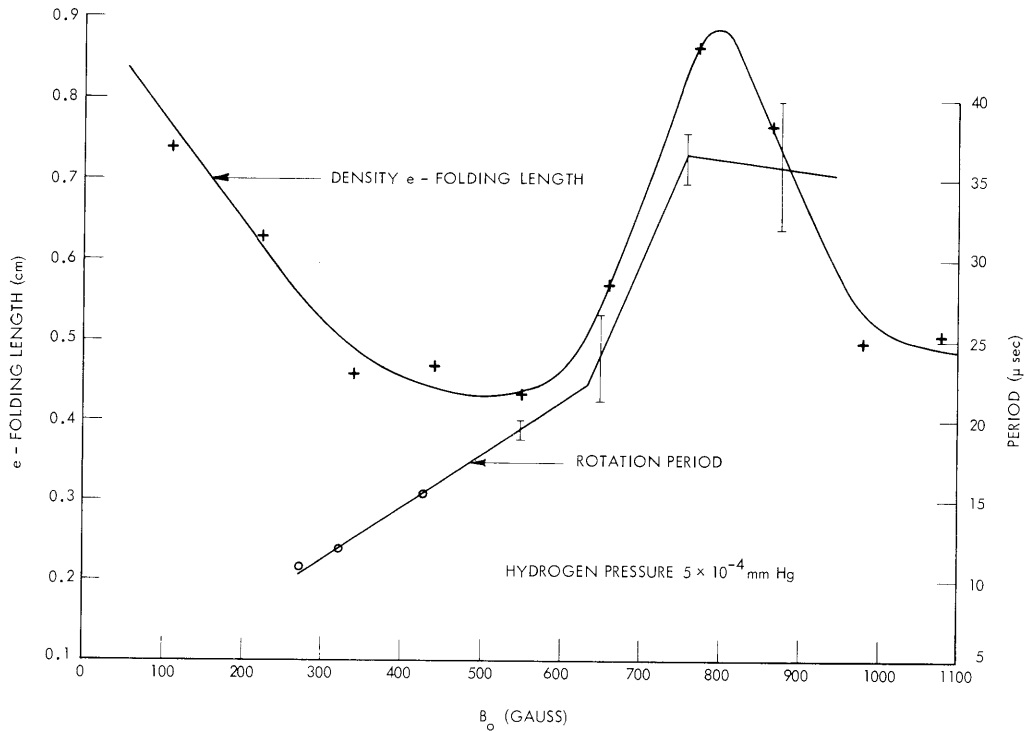


Fig. XVI-10. Density e-folding length and rotation period.

increases sharply. A decrease in net ion current to the wall electrodes at high fields is caused by a change in the potentials in the plasma, not by a decrease in particle flux. Above 1400 gauss the wall electrodes collect net electron current. Biased probes near the wall show that the ion density does not change much as the magnetic field is increased.

The existence of the rotation does not depend directly on the electron beam. After the beam is turned off, the plasma continues to rotate for several periods.

The transport of plasma across the magnetic field appears to be caused by an azimuthal electric field. Electric probe measurements show that the leading edge of the plasma spoke is negative with respect to the trailing edge. The resulting electric field is in such a direction that neutral plasma drifts radially outward. It is thought that the azimuthal electric field is caused by the difference between the electron and ion Hall mobilities. The inward electric field needed to drive the plasma in a right-handed rotation is thought to be caused by the trapping of a hot electron plasma in the magnetic mirror.

B. A. Hartenbaum

References

1. B. A. Hartenbaum, Beam-plasma discharges. System B: Rotational instability and quenching, Quarterly Progress Report No. 70, Research Laboratory of Electronics, M. I. T., July 15, 1963, pp. 111-113.

2. L. D. Smullin, W. D. Getty, B. A. Hartenbaum, and H. Y. Hsieh, Electron beam-plasma interaction experiments, Quarterly Progress Report No. 66, Research Laboratory of Electronics, M. I. T., July 15, 1962, p. 121.

B. ROTATING PLASMA INSTABILITIES

This study has been completed and the results are being prepared for submission to the Department of Electrical Engineering, M. I. T., as a doctoral thesis.

D. L. Morse

C. INSTABILITIES AND AMPLIFYING WAVES IN BEAM PLASMA SYSTEMS

This research has been completed and a doctoral thesis is being prepared for submission to the Department of Electrical Engineering, M. I. T.

R. J. Briggs

D. BEAM-EXCITED ION-PLASMA OSCILLATIONS

Recently, we have found theoretically that a beam of charged particles can interact with the ions of a plasma at the ion-plasma frequency, provided that the electron temperature of the plasma is sufficiently high. It is likely that such an interaction is the mechanism responsible for the VHF oscillations (100-800 mc) observed in the beam-plasma discharge.

We hope to get more direct experimental evidence of this interaction in the apparatus described here. A cyclotron discharge is excited by a 3-kmc power source in a multimode cavity placed in a magnetic mirror. The cavity is continuously pumped, and the gas pressure in the cavity can be regulated. Such a cyclotron discharge can produce a very hot electron gas. The temperature, however, is probably anisotropic with its largest components perpendicular to the magnetic field. Since the magnetic field is inhomogeneous, we may expect part of the transverse random energy to be transferred into the longitudinal direction.

An electron beam is launched into the cyclotron discharge along the axis of the magnetic bottle. The beam is provided by a tantalum cathode heated by electron bombardment from a second, directly heated, W cathode. The gun operates with perveance $I_0/V_0^{3/2} \approx 1-2 \times 10^6$.

Both the discharge and the beam have been operated, but in the early experiments we still have not found any evidence of interaction. The next steps are (i) to increase

(XVI. PLASMA ELECTRONICS)

the microwave heating power from 50 watts to several hundred watts in order to provide a hotter and denser plasma; and (ii) to modulate the beam in the expected frequency band for the ion-plasma frequency (40-100 mc) in order to get a more sensitive test of interaction.

M. T. Vlaardingerbroek, M. A. Lieberman, L. D. Smullin

E. COUPLING OF EMPTY-WAVEGUIDE AND QUASI-STATIC MODES IN WAVEGUIDES LOADED WITH GYROTROPIC MEDIA

In a previous report we presented a new approach to the solution of wave propagation in gyrotropic waveguides.¹ We have since reformulated the coupled equations, so that the coupling between the various modes becomes more obvious. In this report we present the reformulated coupled equations, discuss the coupling between the various modes, and give the results of the numerical calculations for the example partially treated in our previous report, which was for a completely filled, circular, cold, plasma waveguide; the motion of ions is included.

1. Coupled-Mode Theory

We consider a gyrotropic medium characterized by dielectric and magnetic permittivity tensors given by Eqs. 1 and 2 of our previous report.¹ We analyze \bar{E} and \bar{H} in a rotational and an irrotational part according to Eqs. 3a and 3b given there.¹

The orthogonality relations for electrostatic modes are

$$\int_A K_{\parallel} \Phi_{\ell} \Phi_m^* da = \delta_{\ell m} \quad (1a)$$

$$\int_A \nabla_T \Phi_m^* \cdot \bar{K}_T \cdot \nabla_T \Phi_{\ell} da = \gamma_{\ell}^2 \delta_{\ell m}. \quad (1b)$$

Here, the integration is taken over the cross section of the waveguide. In this report a double-bar superscript denotes a tensor, and [] denotes a matrix.

The orthogonality relations for magnetostatic modes are

$$\int_A L_{\parallel} \Psi_m \Psi_{\ell}^* da = \delta_{\ell m} \quad (2a)$$

$$\int_A \nabla_T \Psi_{\ell}^* \cdot \bar{L}_T \cdot \nabla_T \Psi_m da = \gamma_m^2 \delta_{\ell m}. \quad (2b)$$

We define

$$\hat{E}^r = \sum_i (V_i \hat{e}_{Ti} + I_i Z_i \hat{e}_{zi}) \quad (3a)$$

$$\hat{H}^r = \sum_i (I_i \hat{h}_{Ti} + V_i Y_i \hat{h}_{zi}) \quad (3b)$$

$$\Phi = \sum_m F_\ell \Phi_\ell \quad (4)$$

$$\Psi = \sum_m M_m \Psi_m. \quad (5)$$

Substituting Eqs. 3-5 in Maxwell's equations and applying the orthogonality relations, we obtain

$$\gamma \bar{V} - [\Gamma_N][Z] \bar{I} = [a] \bar{I} + [b] \bar{M} \quad (6a)$$

$$\gamma \bar{I} - [\Gamma_N][Y] \bar{V} = [c] \bar{V} + [d] \bar{F} \quad (6b)$$

$$(\gamma^2 - [\Gamma_L][\Gamma_L]) \bar{F} = \left(\frac{[d]}{j\omega\epsilon_0} \right)^\dagger \bar{V} - \gamma [e] \bar{I} \quad (7)$$

$$(\gamma^2 - [\Gamma_M][\Gamma_M]) \bar{M} = -\gamma [f] \bar{V} + \left(\frac{[b]}{j\omega\mu_0} \right)^\dagger \bar{I}. \quad (8)$$

Here, the dagger indicates complex conjugate of the transpose of a matrix, and

$$a_{in} = j\omega\mu_0 \int_A \hat{h}_{Ti}^* \cdot (\bar{\bar{L}}_T - \bar{\bar{I}}_T) \cdot \hat{h}_{Tn} da \quad (9a)$$

$$b_{im} = j\omega\mu_0 \int_A \hat{h}_{Ti}^* \cdot \bar{\bar{L}}_T \cdot (-\nabla_T \Psi_m) da \quad (9b)$$

$$c_{in} = j\omega\epsilon_0 \int_A \hat{e}_{Ti}^* \cdot (\bar{\bar{K}}_T - \bar{\bar{I}}_T) \cdot \hat{e}_{Tn} da \quad (9c)$$

$$d_{i\ell} = j\omega\epsilon_0 \int_A \hat{e}_{Ti}^* \cdot \bar{\bar{K}}_T \cdot (-\nabla_T \Phi_\ell) da \quad (9d)$$

$$e_{\ell i} = \frac{p_{ei}^2}{j\omega\epsilon_0} \int_A K_{\parallel} \Phi_{\ell}^* \phi_i \, da \quad (9e)$$

$$f_{mi} = \frac{p_{hi}^2}{j\omega\mu_0} \int_A L_{\parallel} \Psi_m^* \psi_i \, da. \quad (9f)$$

Lower-case letters for potentials denote the empty-waveguide modes, and upper-case letters, the quasi-static modes. The symbol p denotes transverse wave numbers.

$[\Gamma_N]$ = diagonal matrix for the longitudinal wave numbers of empty-waveguide modes

$[\Gamma_L]$ = corresponding matrix for the electrostatic modes

$[\Gamma_M]$ = corresponding matrix for the magnetostatic modes.

2. Discussion

The dispersion equation of the coupled system may be derived easily from Eqs. 6-8. These equations show which modes have a dominant contribution in the coupling. The left-hand sides of these equations contain the differences $\gamma^2 - \gamma_i^2$. The right-hand sides contain the coupling coefficients. The coupling coefficients depend upon the interaction of the transverse fields of the coupled modes. When the transverse wave numbers of the coupled modes approach each other, the transverse fields of these modes tend to become similar, and therefore the corresponding coupling coefficient increases significantly.

Let us assume that the longitudinal wave numbers and the transverse wave numbers of several modes have large differences. Then the coupling coefficients are small and the difference $\gamma^2 - \gamma_i^2$ for the i^{th} mode is very large. Therefore we may factor $\gamma^2 - \gamma_i^2$ out of the dispersion relation, and this fact, of course, means that the i^{th} mode is not coupled to all of the other modes. If either the longitudinal wave numbers or the transverse wave numbers are close together, the differences $\gamma^2 - \gamma_i^2$ are of the same order or less than the coupling coefficients. In that case $\gamma^2 - \gamma_i^2$ cannot be factored out of the dispersion relation any longer and the i^{th} mode is coupled to the other modes.

3. Example

We consider a completely filled, circular, cylindrical, cold, plasma waveguide of radius a . The quasi-static mode QS_{10} has a transverse wave number $p = \frac{2.405}{a}$. Therefore there is a strong coupling between this quasi-static mode and the empty-waveguide mode TM_{10} which has the same transverse wave number. The mode QS_{10} is also coupled to the TE_{10} ($p = 3.83/a$) because their transverse wave numbers are close. For $\frac{\omega a}{c} > 4$ there is a strong coupling between the modes TE_{10} and QS_{10} because their longitudinal wave numbers are extremely close. The resulting dispersion diagram is

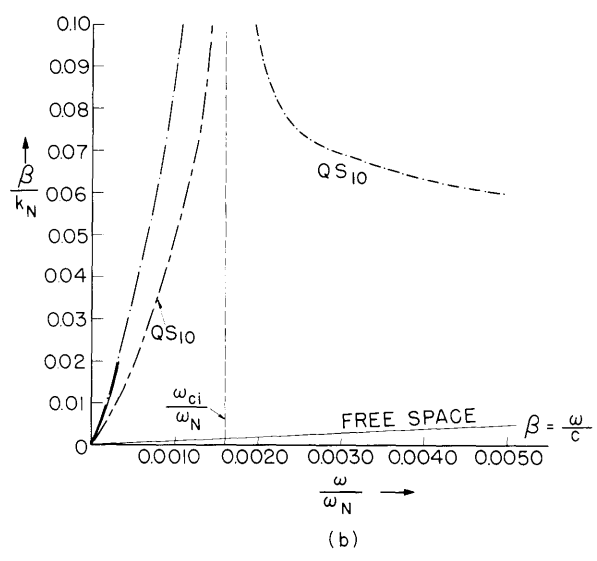
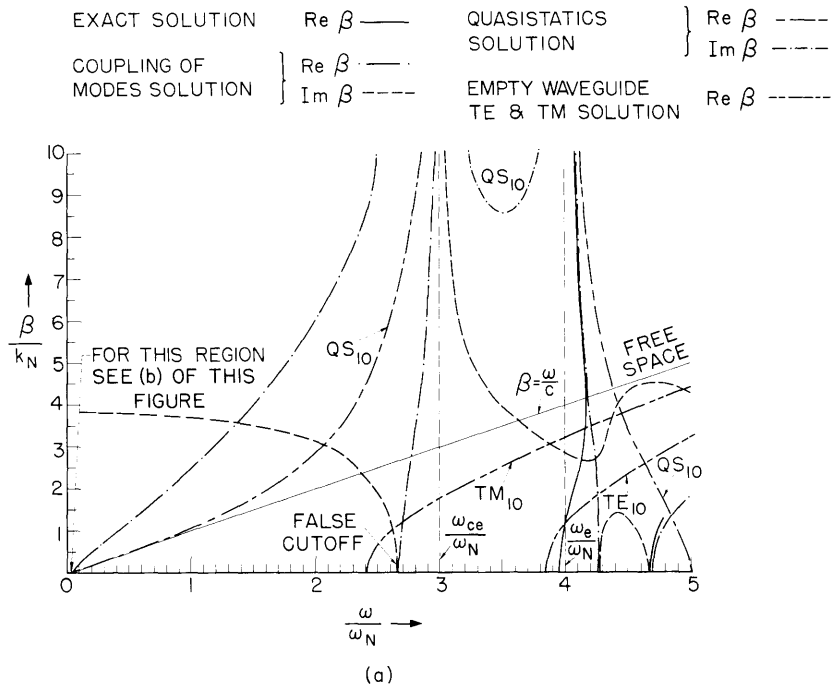


Fig. XVI-11. Dispersion diagrams for plasma-filled waveguide, $\omega_n = c/a$, $k_n = 1/a$, where a is the radius of the waveguide. For comparison, we show the solutions from quasi-static theory, exact theory, and coupling-of-modes theory, together with the uncoupled modes. (a) Frequency regime from the first cutoff above ω_{ci} . The second branch from coupling of modes is imaginary and similar to that of QS_{10} but with $(\beta/k_N)_{\min} \approx 12.4$. (b) Low-frequency regime near and below ω_{ci} . The first branch from coupling of modes for $\omega > \omega_{ci}$ is imaginary, and it is out of the figure because $\beta/k_N > 10$ for $\omega_{ci}/\omega_N < \omega/\omega_N < 0.0050$. Its shape is similar to that of QS_{10} . The second root from coupling-of-modes theory is imaginary, and is given by $\approx +j3.83$ from $\omega/\omega_N = 0$ to $\omega/\omega_N = 0.1$. See (a).

shown in Fig. XVI-11. For comparison we have also shown in Fig. XVI-11 the known part of the exact dispersion diagram and the dispersion curve obtained under the quasi-static approximation.

A study of these dispersion curves shows that by use of the coupled-mode theory we significantly improve the quasi-static curve, and thus we obtain an extremely good approximation to the exact solution. We should notice that the couplings are due to the fact that the corresponding modes have longitudinal and/or transverse wave numbers very close to each other. Note that the coupling between the TM_{10} and QS_{10} modes produces strong effects on the dispersion diagram for all frequencies. This is due to the fact that the transverse wave numbers of these modes are identical for all frequencies, even though the longitudinal wave numbers are close only near plasma resonance.

The coupling of modes will, however, introduce extraneous solutions. These arise because (i) we have expanded the fields in a redundant (more than complete) set, and (ii) we use only a few of the modes that appear to be coupled strongest. Thus in our example, the approximate equation for the H-cutoffs¹ has a solution at $(\omega/\omega_n) = 2.63$. This is a false cutoff,² and hence the branch of β that starts from there must be disregarded. In general, the extraneous branches of β can be detected, since we have a means of obtaining the exact solutions at the cutoffs, near the resonances, and at very low frequencies.²

4. MHD Regime Approximation

Very good approximations to the exact solution have been given for cutoffs, resonances, and the very low frequency region (magnetohydrodynamic region).² In our previous report¹ we have shown that the coupled-mode theory provides results that are almost identical to the approximations given by Bers for resonances and cutoffs.² The same holds true for the magnetohydrodynamic region, as we show below.

By taking into consideration the fact that for very low frequencies $\omega^2 \rightarrow 0$ and $K_{\parallel} \rightarrow -\infty$ so that $\omega^2 K_{\parallel}$ is finite, the dispersion equation (13) of our previous report¹ yields

$$\gamma^2 = p_{h1}^2 - k_o^2 K_{\perp} \quad (10a)$$

$$\gamma^2 = \frac{K_{\perp}}{K_{\parallel}} p_{e1}^2 - k_o^2 K_{\perp}, \quad (10b)$$

which are identical to the approximate expressions for the magnetohydrodynamic region given by Bers.²

P. E. Serafim, A. Bers

References

1. P. E. Serafim and A. Bers, Coupling of empty-waveguide modes, electrostatic and magnetostatic modes in waveguides loaded with gyrotropic media, Quarterly Progress Report No. 69, Research Laboratory of Electronics, M.I.T., April 15, 1963, pp. 57-61.
2. W. P. Allis, S. J. Buchsbaum, and A. Bers, Waves in Anisotropic Plasmas (The M. I. T. Press, Cambridge, Mass., 1963), Chapter 9.

F. TURBULENT DIFFUSION ACROSS A MAGNETIC FIELD

1. Theory

It has been observed that the plasma columns generated by hollow-cathode arcs in our laboratory, and by other mechanisms elsewhere, exhibit large spatial and temporal fluctuations, and that the diffusion across the magnetic field often substantially exceeds that predicted by quiescent diffusion theory. Besides the well-known short-circuit end effect of "Simon" diffusion,¹ we must consider the effects of turbulent diffusion. In this report we consider an elementary model of the process, and the experimental evidence that supports it.

We presume that the plasma column has many unstable modes, whose origins we cannot properly determine, and that the resulting turbulence leads to an axial shredding of the plasma column, that is, density, potential, and so forth, are well correlated along magnetic-field lines, but are poorly correlated across field lines; this has been observed experimentally. These plasma strings move randomly at the stochastic $\underline{E} \times \underline{B}/B^2$ velocities across field lines.

A radial diffusion coefficient for these plasma strings can be conceptually defined as

$$D = \langle L_r V / 3 \rangle. \quad (1)$$

Here, L_r is the radial distance that the string travels before a change in direction and is associated with the radial correlation length for plasma fluctuations. The speed V is

$$V = |E_\theta / B|. \quad (2)$$

From the magnitude of the fluctuating component ϕ of the plasma potential, we can obtain the random azimuthal electric field

$$|E_\phi| = |\phi / L_\theta|. \quad (3)$$

Here, L_θ is the distance over which it develops. Thus, apart from averaging coefficients of order one, we have

$$D \approx \langle L_r |\phi| / 3BL_\theta \rangle. \quad (4)$$

Equation 4 has the form of anomalous or "Bohm" diffusion.

We now argue heuristically that if there are many turbulent modes and none dominates, the correlation lengths will all be the same. The plasma strings are of radial size L_r ; as they move and collide at random, they are polarized by their motion (or vice versa). Hence the radial correlation lengths for density and potential will be the same. The r versus θ correlation equalities are less clear. But we propose that even though the plasma rotates about the axis and may have a quasi-coherent rotating structure, the azimuthal motion does not of itself lead to radial diffusion. We presume (and evidence similar to that given below tends to bear us out) that within these organized motions, a θ -turbulence exists with approximately the same time and scale lengths. From these considerations, we have

$$D \approx \langle |\phi| / 3B \rangle, \quad (5)$$

a result that can be checked by measuring fluctuating potential amplitudes, radial flows, and radial mean-density gradients. Also, if correlations over a length L last a time t , we can write

$$L = Et/b, \quad (6)$$

and hence

$$L = \langle |\phi| t / B \rangle^{1/2}, \quad (7)$$

apart from factors of order one. Equation 5 can be expected to have validity in cases in which the turbulent diffusion greatly exceeds the classical rate.

2. The Experiment

The hollow-cathode arc described in detail by Alvarez de Toledo^{2,3} was used. The plasma column, ≈ 1.5 m long, ran down the lines of magnetic induction, through a magnetic mirror (mirror ratio, 2.5). Other parameter ranges were: arc current, 15-35 amp; pressure, 10^{-4} - 1.5×10^{-3} Torr; midplane induction, 0.025-0.11 weber/m². The plasma column was bounded axially by insulating end plates; thus the radial and azimuthal electric fields were not shorted out.

Plane and cylindrical Langmuir probes through ball joints, or on a sliding axial rail, were used to measure ion saturation current (to obtain ion density), and to measure floating potential. Occasional measurements of electron saturation current always correlated well with ion saturation current. Thus floating-potential fluctuations, which were found to be uncorrelated with density except when organized rotation was present, were assumed to indicate the fluctuating potential ϕ .

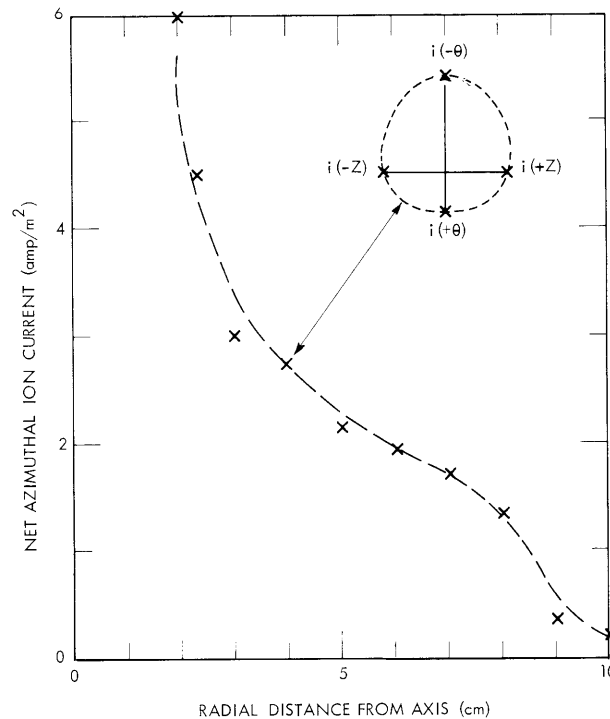


Fig. XVI-12. Net azimuthal ion current vs radial distance. Inset shows the current profile at $r = 4$ cm from directions normal to some radius. Thus $i(\pm\theta)$ are azimuthal currents and $i(\pm z)$ are axial currents. Note the approximate axial symmetry. Arc current, 20 amp; $B = 0.105$ weber/m²; $p = 1.3 \times 10^{-3}$ Torr.

To a first approximation, the mean azimuthal ion current can be measured with plane Langmuir probes sensitive to the arrival of particles from the $\pm\theta$ directions. Then

$$eA\Gamma_{\theta} = i_{+s}(+\theta) - i_{+s}(-\theta). \quad (8)$$

Here, Γ_{θ} is net azimuthal current density, A is the probe area, and $i_{+s}(\pm\theta)$ are the ion saturation currents with the probe oriented in each direction. With the probes oriented, we observed an azimuthal flow comparable in magnitude to the radial current, whose value is estimated below. The flow is in the $\underline{E} \times \underline{B}$ direction, with \underline{E} pointing toward the arc axis. Figure XVI-12 shows the net current for a typical case.

In some instances, data taken with two midplane probes at different azimuths showed a spiral-like structure in the plasma, as in Fig. XVI-13. Simple turbulent diffusion theory did not fit these cases.

In principle, the net radial current could be measured by examining $i_{+s}(\pm r)$, but a probe with the required movements was not available. Thus the radial ion saturation current density was measured at the wall, radius r_w ; the current density at radius r is

(XVI. PLASMA ELECTRONICS)

$$i_r(r) = i_r(r_w)(r_w/r), \tag{9}$$

if no sources or sinks are present.

The electron temperature was measured and was found to decrease with radius, being 1-3 ev near the core, and 0.25-0.5 ev at $r = 10$ cm. Figure XVI-14 shows a temperature

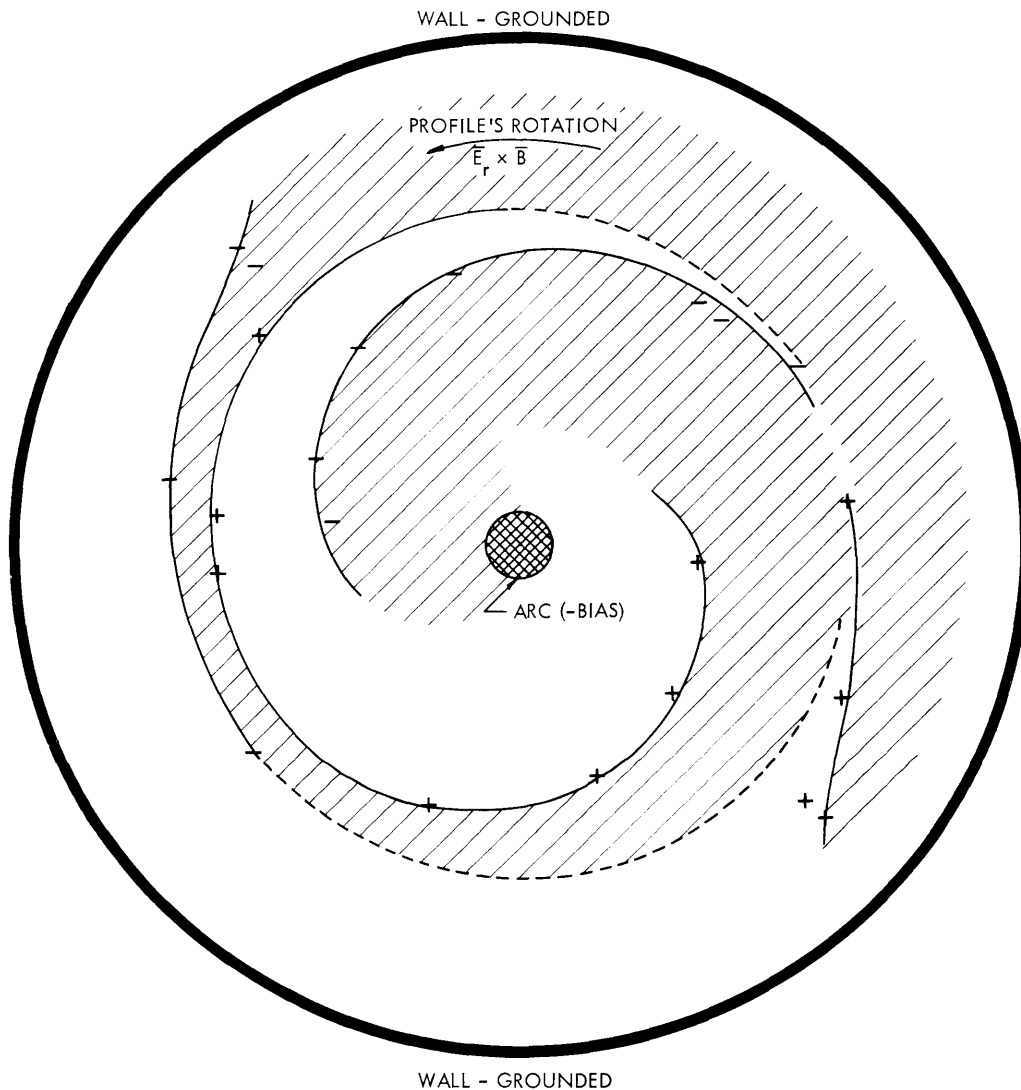


Fig. XVI-13. Plasma spiral structure with rotational instability. The negative space-charge front (-) and positive space-charge tail (+) are shown. Arc current, 35 amps; $B = 0.055$ weber/m²; $p = 6 \times 10^{-4}$ Torr.

profile similar to those obtained by Rothleder.⁴ The profile remained similar for all of our runs, except for the absolute ordinate scale. Therefore the same profile,

renormalized for each run at $r = 4$ cm, was used for the subsequent calculations.

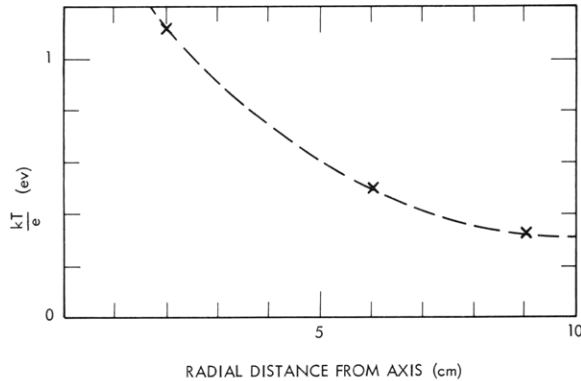


Fig. XVI-14.

Electron temperature as a function of radius. Arc current, 20 amps; $B = 0.024$ weber/m²; $p = 1 \times 10^{-4}$ Torr.

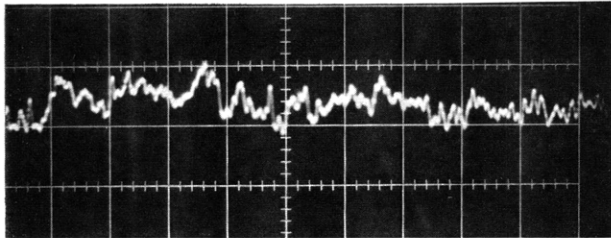


Fig. XVI-15.

Floating potential vs time. Vertical scale, 0.5 V/cm; horizontal scale, 200 μ sec/cm. Probe at $r = 6$ cm. Arc current, 20 amps; $B = 0.024$ weber/m²; $p = 1 \times 10^{-4}$ Torr; $T_- = 0.5$ eV.

The fluctuating potential ϕ , as a substitute for plasma potential, was photographed on an oscilloscope. Figure XVI-15 shows a typical trace.

3. Results

The diffusion current is

$$\Gamma = -\nabla(dn). \quad (10)$$

Then, for the turbulent diffusion, we have a radial ion current density

$$\Gamma_{+r} = -\frac{\partial}{\partial r} \left[\frac{\langle |\phi| \rangle n_+}{3B} \right]. \quad (11)$$

But

$$n_+ = j_{+s} / e \left[\frac{eT_-}{2.7m_+} \right]^{1/2}, \quad (12)$$

where j_{+s} is the saturation ion current density, m_+ is the ion (argon) mass, and T_- is the electron temperature. Thus the net radial ion current (in amperes)

(XVI. PLASMA ELECTRONICS)

should be given by

$$i_{+r} = - \left(\frac{0.27 m_+^{1/2}}{B} \right) \frac{\partial}{\partial r} \left[\frac{\langle |\phi| \rangle i_{+s}}{T_-^{1/2}} \right]. \quad (13)$$

Figure XVI-16 shows the two sides of Eq. 13 plotted against radial distance. The points are derived from the formula on the right-hand side of Eq. 13; all quantities are evaluated experimentally at each point. The shaded region is obtained from the wall current and

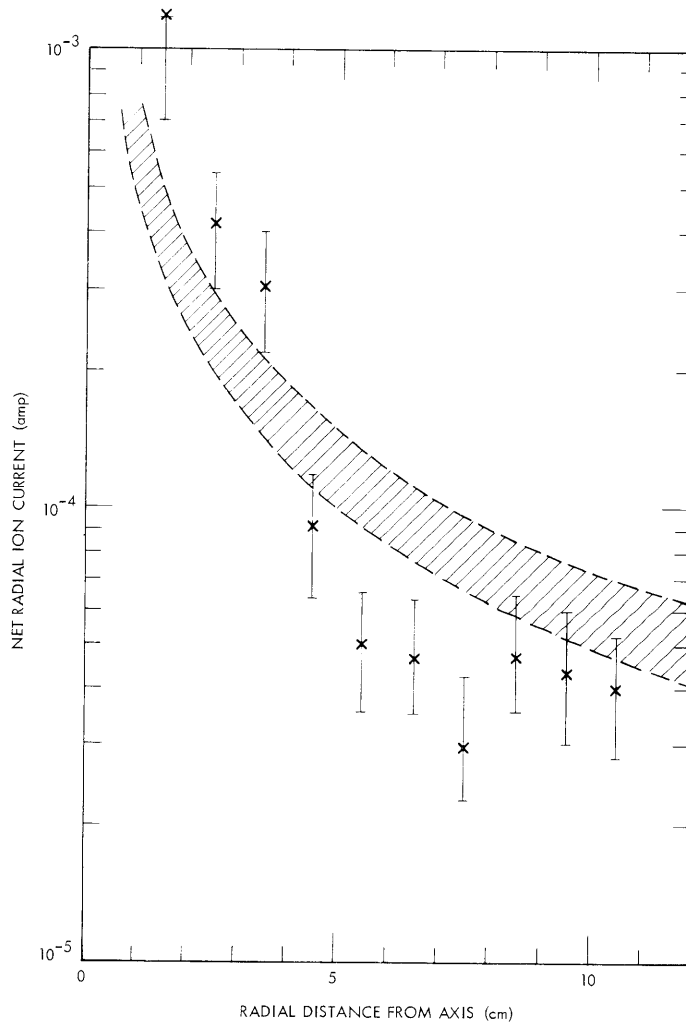


Fig. XVI-16. Net radial current vs radial position. Shaded area, evaluation of left-hand side of Eq. 13; points, evaluation of right-hand side of Eq. 13. Arc current, 20 amps; $B = 0.105$ weber/m²; $p = 1.3 \times 10^{-3}$ Torr; probe area, ~ 4 mm².

Eq. 9, and includes an experimental error estimate. If we take into consideration the crudity of the theory and the experimental difficulty of measuring the various quantities (particularly the fluctuating potential and its average), the agreement is tolerable. Classical nonturbulent theory predicts radial currents approximately two orders of magnitude smaller.

We can make a few additional remarks pertaining to the applicability of a stochastic theory to the plasma motions. First, from visual inspection of simultaneous potential or density fluctuation on different B lines, a rough estimate of the autocorrelation in distance and time can be made. Equation 7 was found to be accurate within a factor of ~ 2 . Also, the theory of Yoshikawa and Rose,⁵ for example, predicts that the density fluctuations should represent almost 100 per cent modulation in cases for which $\langle |\phi| \rangle$ is comparable to kT_e/e . Experimentally, this was observed to be the case.

F. Alvarez de Toledo, D. J. Rose

References

1. A. Simon, An Introduction to Thermonuclear Research (Pergamon Press, New York, 1959), pp. 150 ff.
2. F. Alvarez de Toledo, S. M. Thesis, Department of Nuclear Engineering, M. I. T., 1963.
3. F. Alvarez de Toledo, N. E. Report, Department of Nuclear Engineering, M. I. T., 1963.
4. S. D. Rothleder, Ph. D. Thesis, Department of Nuclear Engineering, M. I. T., 1962.
5. S. Yoshikawa and D. J. Rose, Anomalous diffusion of a plasma across a magnetic field, Phys. Fluids 5, 334-340 (1962).

